arXiv:1806.09781v2 [astro-ph.CO] 4 Oct 2018

MODEL-INDEPENDENT CURVATURE DETERMINATION FROM GRAVITATIONAL-WAVE STANDARD SIRENS AND COSMIC CHRONOMETERS

Jun-Jie Wei[1,2]

[1] Purple Mountain Observatory, Chinese Academy of Sciences, Nanjing 210008, China; jjwei@pmo.ac.cn
[2] Guangxi Key Laboratory for Relativistic Astrophysics, Guangxi University, Nanning 530004, China
Draft version October 5, 2018

ABSTRACT

The detection of gravitational waves (GWs) provides a direct way to measure the luminosity distance, which enables us to probe cosmology. In this paper, we continue to expand the application of GW standard sirens in cosmology, and propose that the spatial curvature can be estimated in a model-independent way by comparing the distances from future GW sources and current cosmic-chronometer observations. We expect an electromagnetic counterpart of the GW event to give the source redshift, and simulate hundreds of GW data from the coalescence of double neutron stars and black hole–neutron star binaries using the Einstein Telescope as reference. Our simulations show that, from 100 simulated GW events and 31 current cosmic-chronometer measurements, the error of the curvature parameter Ω_K is expected to be constrained at the level of ~ 0.125. If 1000 GW events are observed, the uncertainty of Ω_K would be further reduced to ~ 0.040. We also find that adding 50 mock $H(z)$ data (consisting of 81 cosmic-chronometer data and 1000 simulated GW events) could result in much tighter constraint on the zero cosmic curvature, for which, $\Omega_K = -0.002 \pm 0.028$. Compared to some actual model-independent curvature tests involving the distances from other cosmic probes, this method with GW data achieves constraints with much higher precision.

Subject headings: cosmological parameters — cosmology: observations — gravitational waves — galaxies: general

1. INTRODUCTION

The spatial curvature of the universe is one of the important research topics in modern cosmology. To be specific, estimating the cosmic curvature is an effective way to test the fundamental assumption that the universe is well described by the homogeneous and isotropic Friedmann–Lemaître–Robertson–Walker (FLRW) metric. Note that the possible invalidation of the FLRW approximation has been suggested to explain the accelerated expansion of the universe (e.g., Ferrer & Räsänen 2006; Enqvist 2008; Ferrer et al. 2009; Räsänen 2009; Boehm & Räsänen 2013; Lavinto et al. 2013; Redlich et al. 2014). On the other hand, even if the FLRW metric is valid, whether the cosmic space is open, flat, or closed is crucial for us to understand the evolution of our universe and the nature of dark energy (Ichikawa & Takahashi 2006; Ichikawa et al. 2006; Clarkson et al. 2007; Gong & Wang 2007; Virey et al. 2008; Zolnierowski & Blanchard 2015). Any significant deviation from the zero cosmic curvature would have far-reaching consequences for fundamental physics and inflation models (Eisenstein et al. 2005; Tegmark et al. 2006; Wright 2007; Zhao et al. 2007). Although a spatially flat Universe ($\Omega_K = 0$) is strongly supported by various cosmological probes, especially by the latest *Planck* 2015 results of observations of the cosmic microwave background (CMB; Planck Collaboration et al. 2016),[1] most of the curvature constraints are not in a direct geometric way. That is, some specific cosmological models (e.g., the standard ΛCDM

model) are assumed in a determination of the curvature, thus these results are indirect and cosmological-model-dependent. Besides, because of the strong degeneracy between the cosmic curvature Ω_K and the dark energy equation of state w, it is difficult to constrain the two parameters simultaneously in a non-flat wCDM model. Therefore, it would be better to measure spatial curvature by purely geometrical and model-independent methods.

In Bernstein (2006), a model-independent determination of the curvature parameter Ω_K based on the sum rule of distances along null geodesics of the FLRW metric was presented (see also Knox 2006). Recently, this distance sum rule was put forward to test the FLRW metric and estimate the curvature by using the Union2.1 compilation of type Ia supernovae (SNe Ia) and strong gravitational lensing systems observed from the Sloan Lens ACS Survey (Räsänen et al. 2015). However, the spatial curvature was weakly constrained due to the large uncertainties in the gravitational lensing data. Following the method of Räsänen et al. (2015), the null test of the curvature has been carried out with updated observations (Liao et al. 2017a; Xia et al. 2017; Li et al. 2018; Qi et al. 2018). Based on this distance sum rule, Denissenya et al. (2018) recently employed strong lensing time delays and supernova distances to measure the curvature, and estimated uncertainties on the curvature enabled by future survey data. Another model-independent method was proposed to determine Ω_K by combining measurements of the Hubble parameter $H(z)$ and the luminosity distance $D_L(z)$ (or the angular diameter distance $D_A(z)$) (Clarkson et al. 2007, 2008):

$$\Omega_K = \frac{\left[H(z)D'(z)\right]^2 - 1}{\left[H_0 D(z)\right]^2} \,, \qquad (1)$$

where H_0 is the Hubble constant, $D(z) = (1 + z)D_A(z) = D_L(z)/(1+z)$ represents the comoving angular diameter dis-

tance, and $D'(z) = dD(z)/dz$ denotes the derivative with respect to redshift z. This method have been extensively used in the literature (Shafieloo & Clarkson 2010; Mortsell & Jonsson 2011; Sapone et al. 2014; Li et al. 2014; Yahya et al. 2014; Cai et al. 2016; L'Huillier & Shafieloo 2017; Rana et al. 2017). However, in this method, the derivative of comoving distance with respect to z is necessary to estimate the curvature, which introduces a considerable uncertainty. Recently, stricter constraints on the curvature from measurements of expansion rate and distance have been obtained by dodging the derivative of distance with respect to z (Li et al. 2016; Yu & Wang 2016; Cao et al. 2017; Wang et al. 2017; Wei & Wu 2017a; Yu et al. 2018). In addition to these above two methods, there has been some other works proposing model-independent methods to determine the curvature and some approaches to reduce the measurement sensitivity of Ω_K to dark energy (e.g., Takada & Doré 2015; Witzemann et al. 2018). For example, Takada & Doré (2015) estimated a best achievable accuracy of the curvature constraint with the radial and angular diameter distances from future baryon acoustic oscillation experiments. Witzemann et al. (2018) showed that forthcoming 21 cm intensity mapping experiments are ideally designed to carry out curvature determinations, as they can detect the clustering signal at high redshift with sufficient precision to break the degeneracy of dark energy and curvature.

On the other hand, the joint detection of the gravitational-wave (GW) event GW170817 with electromagnetic (EM) counterparts (e.g., a gamma-ray burst GRB 170817A, or a kilonova) from the merger of binary neutron stars (NSs) (Abbott et al. 2017a; Coulter et al. 2017; Goldstein et al. 2017) has opened the new era of multi-messenger cosmology (Abbott et al. 2017b). The application of GWs in cosmology was first suggested by Schutz (1986), who proposed that the Hubble constant can be determined from GW observations, since the waveform signals of GWs from inspiralling and merging compact binaries encode distance information (see also Holz & Hughes 2005; Messenger et al. 2014; Zhao & Wen 2018). Thus, GWs can serve as standard sirens, analogous to SN standard candles. But, unlike the distance calibration of SNe Ia that rely on the nuisance parameters characterizing SN light-curves, the GW standard-siren observations can measure the luminosity distances directly, without the need of any other cosmic distance ladders (i.e., they are self-calibrating). This advantage of GWs can help us dodge the influence of the nuisance parameters on the test of the curvature, which should be considered when one makes use of the SNe Ia data (Li et al. 2016; Wei & Wu 2017a). Therefore, combining $H(z)$ and GW data provides a novel way to determine the cosmic curvature.

In the past, the simulated GW data have been used to measure the cosmological parameters (e.g., Holz & Hughes 2005; Zhao et al. 2011; Del Pozzo 2012; Cai et al. 2016; Del Pozzo et al. 2017; Liao et al. 2017b; Wei & Wu 2017b; Wei et al. 2018), test the cosmic distance duality relation (Yang et al. 2017), weigh the total neutrino mass (Wang et al. 2018), explore the anisotropy of the universe (Cai et al. 2018; Lin et al. 2018), and constrain the time variation of Newton's constant G (Zhao et al. 2018). We note that one recent work (Jimenez et al. 2018) provided an analysis of curvature constraints in a model-independent way using distance probes: GWs, cosmic chronometers, and redshift drift. They discussed what kind of observations and what level of uncertainty will be needed to measure the curvature at the CMB

fluctuations level of $\sim 10^{-5}$, and found that one could measure the curvature at the desired accuracy only when improving the uncertainties on the Hubble parameter and the luminosity distance from the GW source by a factor of 10 and 1000, respectively. In this paper, following the method proposed in Clarkson et al. (2007, 2008), we investigate what level of curvature constraints can be achieved using future GW data in the era of the third-generation GW detectors such as the Einstein Telescope (ET). The uncertainty on the GW luminosity distance is adopted as the designed level of the ET. Firstly, using a non-parametric smoothing technique, we reconstruct a continuous $H(z)$ function from measurements of the expansion rate from cosmic chronometers. The model-independent comoving distance can then be directly obtained by integrating the reconstructed $H(z)$ function. Next, with the curvature parameter Ω_K taken into account, we transform the comoving distance into the curvature-dependent luminosity distance D_L^H. Finally, by comparing $D_L^H(z)$ to the luminosity distances $D_L^{GW}(z)$ derived from the mock GW data, we achieve a cosmology-independent and compelling test of the cosmic curvature.

The paper is arranged as follows. In Section 2, we derive the luminosity distance information D_L^H and D_L^{GW} from expansion rate measurements and GW standard sirens, respectively. In Section 3, we demonstrate that an accurate determination of the curvature parameter can be achieved in a model-independent way by confronting D_L^H with D_L^{GW}, using Monte Carlo simulations. Lastly, we give a brief summary and discussion in Section 4. Throughout this paper, the geometric unit $G = c = 1$ is adopted.

2. METHOD DESCRIPTION

2.1. *Distance from Cosmic-Chronometer Measurements*

Since the expansion rate of the universe relates to the expansion factor $a(t)$, i.e., $H(z) \equiv \dot{a}/a$, $H(z)$ can be directly measured from the time-redshift derivative dt/dz using $H(z) = -\frac{1}{1+z}\frac{dz}{dt}$. That is, the Hubble parameter $H(z)$ can be obtained in a cosmology-independent way by calculating the differential age evolution of passively evolving galaxies (Jimenez & Loeb 2002). In the literature, these galaxies are usually called cosmic chronometers. We use the most complete sample of 30 cosmic-chronometer measurements that obtained from Moresco et al. (2016). We also include a recent cosmic-chronometer measurement at a redshift of $z = 0.47$ (Ratsimbazafy et al. 2017). Our sample now contains 31 data points in the redshift range of $0 < z < 2.0$, which is listed in Table 1.

In our analysis, we use the model-independent smoothing technique, Gaussian process (GP), to reconstruct a continuous $H(z)$ function that best approximates the discrete Hubble parameter data we have compiled in Table 1. There is an open-source Python package of GP called GaPP developed by Seikel et al. (2012a), which is widely used for cosmological studies (e.g., Bilicki & Seikel 2012; Seikel et al. 2012b; Cai et al. 2016; Yu & Wang 2016; Wei & Wu 2017a; Yennapureddy & Melia 2017, 2018; Melia & Yennapureddy 2018). The readers may turn to Seikel et al. (2012a) for detailed information about the GP method and the package GaPP. Using the GP method, the reconstructed $H(z)$ function (solid line) with 1σ and 2σ confidence regions (shaded areas) for 31 discrete $H(z)$ measurements are shown in Figure 1(a). For comparison, we also fit the discrete $H(z)$ data using the flat ΛCDM model. The best-fit cosmological param-

TABLE 1
$H(z)$ Measurements Obtained from the Cosmic-Chronometer
Approach

z	$H(z)$ (km s^{-1} Mpc^{-1})	References
0.09	69 ± 12	Jimenez et al. (2003)
0.17	83 ± 8	
0.27	77 ± 14	
0.4	95 ± 17	
0.9	117 ± 23	Simon et al. (2005)
1.3	168 ± 17	
1.43	177 ± 18	
1.53	140 ± 14	
1.75	202 ± 40	
0.48	97 ± 62	Stern et al. (2010)
0.88	90 ± 40	
0.1791	75 ± 4	
0.1993	75 ± 5	
0.3519	83 ± 14	
0.5929	104 ± 13	Moresco et al. (2012)
0.6797	92 ± 8	
0.7812	105 ± 12	
0.8754	125 ± 17	
1.037	154 ± 20	
0.07	69 ± 19.6	
0.12	68.6 ± 26.2	
0.2	72.9 ± 29.6	Zhang et al. (2014)
0.28	88.8 ± 36.6	
1.363	160 ± 33.6	Moresco (2015)
1.965	186.5 ± 50.4	
0.3802	83 ± 13.5	
0.4004	77 ± 10.2	
0.4247	87.1 ± 11.2	Moresco et al. (2016)
0.4497	92.8 ± 12.9	
0.4783	80.9 ± 9	
0.47	89 ± 50	Ratsimbazafy et al. (2017)

eters are $H_0 = 67.93^{+2.69}_{-2.61}$ km s^{-1} Mpc^{-1} and $\Omega_m = 0.324^{+0.053}_{-0.050}$. The corresponding best-fit theoretical curve is presented in Figure 1(a) with a dashed line. It is obvious that the reconstruction of $H(z)$ is consistent with the best-fit flat ΛCDM model within 1σ confidence region, suggesting that the GP method can provide a reliable reconstructed function from the observed data.

Within the framework of FLRW metric, the line-of-sight comoving distance can be expressed as (Hogg 1999)

$$D_C(z) = \int_0^z \frac{dz'}{H(z')} \ . \tag{2}$$

By integrating the reconstructed $H(z)$ function and its 1σ and 2σ error bars with respect to redshift, we can then derive the model-independent $D_C(z)$ function and the corresponding 1σ and 2σ confidence regions, respectively. As shown in Figure 1(b), the reconstructed $D_C(z)$ function (solid line) is also in good agreement with that determined from the best-fit flat ΛCDM model (dashed line).

With the reconstructed comoving distance function $D_C(z)$ and its 1σ uncertainty σ_{D_C}, the correlated luminosity distance D_L^H from the $H(z)$ data can then be calculated by

$$\frac{D_L^H(z)}{(1+z)} = \begin{cases} \frac{1}{H_0}\frac{1}{\sqrt{|\Omega_K|}} \sinh\left[\sqrt{|\Omega_K|}D_C(z)H_0\right] & \text{for } \Omega_K > 0 \\ D_C(z) & \text{for } \Omega_K = 0 , \\ \frac{1}{H_0}\frac{1}{\sqrt{|\Omega_K|}} \sin\left[\sqrt{|\Omega_K|}D_C(z)H_0\right] & \text{for } \Omega_K < 0 \end{cases} \tag{3}$$
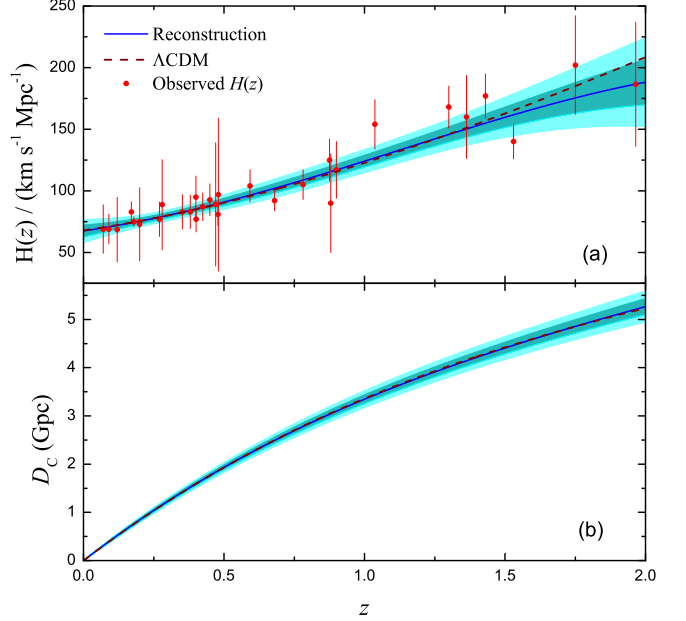

FIG. 1.— Reconstructed Hubble parameter function $H(z)$ (panel (a); solid line) from 31 cosmic-chronometer measurements with the GP method. The corresponding continuous $D_C(z)$ function (solid line) in panel (b) are derived from the reconstruction of $H(z)$. The shadow areas are the 1σ and 2σ confidence regions of the reconstruction. The best-fit flat ΛCDM model (dashed line) with $H_0 = 67.93$ km s^{-1} Mpc^{-1} and $\Omega_m = 0.324$ is also shown.

with its corresponding uncertainty

$$\sigma_{D_L^H} = \begin{cases} (1+z)\cosh\left[\sqrt{|\Omega_K|}D_C(z)H_0\right]\sigma_{D_C} & \text{for } \Omega_K > 0 \\ (1+z)\sigma_{D_C} & \text{for } \Omega_K = 0 , \\ (1+z)\cos\left[\sqrt{|\Omega_K|}D_C(z)H_0\right]\sigma_{D_C} & \text{for } \Omega_K < 0 \end{cases} \tag{4}$$

where we emphasize that the cosmic curvature Ω_K and the Hubble constant H_0 are the only two free parameters.

2.2. Distance from GW Sources

Unlike the distance estimation of SNe Ia that rely on the light curve fitting parameters, the GW signals from inspiralling and merging compact binaries can provide an absolute measure of the luminosity distance D_L^{GW}. If compact binaries are NS–NS binaries or black hole (BH)–NS binaries, the source redshifts may be obtained from EM counterparts that occur coincidentally with the GW events (Nissanke et al. 2010; Sathyaprakash et al. 2010; Zhao et al. 2011; Cai & Yang 2017). Therefore, this provides a model-independent way to construct the D_L^{GW}–z relation. The ET,[2] with ultra-high sensitivity (10 times more sensitive than the current advanced ground-based detectors) and wide frequency range ($1 - 10^4$ Hz), would be able to detect GW signals up to redshift $z \sim 2$ for the NS–NS mergers and $z > 2$ for the BH–NS systems. Here, we forecast the curvature constraints from future GW data using the ET as reference.

To get the uncertainties in the luminosity distance of GW sources, one needs to generate the waveform of GWs. In the transverse-traceless gauge, the detector response to a GW signal is a linear combination of two wave polarizations,

$$h(t) = F_+(\theta, \phi, \psi)h_+(t) + F_\times(\theta, \phi, \psi)h_\times(t) , \tag{5}$$

[2] The Einstein Telescope Project, https://www.et.gw.eu/et/.

where h_+ and $h_\times$ are the plus and cross modes of GW, respectively. The antenna pattern functions F_+ and $F_\times$ depend on the source's position (θ, ϕ), the polarization angle ψ, as well as the detector's location and orientation. The pattern functions of one of the three interferometers in the ET are (Zhao et al. 2011)

$$
\begin{aligned}
F_+^{(1)}(\theta,\phi,\psi) = &\ \frac{\sqrt{3}}{2}[\frac{1}{2}(1+\cos^2(\theta))\cos(2\phi)\cos(2\psi) \\
&- \cos(\theta)\sin(2\phi)\sin(2\psi)], \\
F_\times^{(1)}(\theta,\phi,\psi) = &\ \frac{\sqrt{3}}{2}[\frac{1}{2}(1+\cos^2(\theta))\cos(2\phi)\sin(2\psi) \\
&+ \cos(\theta)\sin(2\phi)\cos(2\psi)].
\end{aligned} \tag{6}
$$

Since these interferometers align with an angle $60°$ with each other, the two others' pattern functions are $F_{+,\times}^{(2)}(\theta,\phi,\psi) = F_{+,\times}^{(1)}(\theta, \phi+2\pi/3, \psi)$ and $F_{+,\times}^{(3)}(\theta,\phi,\psi) = F_{+,\times}^{(1)}(\theta, \phi+4\pi/3, \psi)$, respectively.

Following Sathyaprakash & Schutz (2009) and Zhao et al. (2011), we calculate the Fourier transform $\mathcal{H}(f)$ of the time domain waveform $h(t)$ by applying the stationary phase approximation,

$$
\mathcal{H}(f) = \mathcal{A}f^{-7/6}e^{i\Psi(f)}, \tag{7}
$$

where the Fourier amplitude is given by

$$
\begin{aligned}
\mathcal{A} = &\ \frac{1}{D_L^{\mathrm{GW}}}\sqrt{F_+^2\left(1+\cos^2(\iota)\right)^2 + 4F_\times^2\cos^2(\iota)} \\
&\times \sqrt{5\pi/96}\pi^{-7/6}\mathcal{M}_c^{5/6},
\end{aligned} \tag{8}
$$

where ι is the inclination angle between the binary's orbital and the line-of-sight, and

$$
D_L(z) = \frac{1+z}{H_0}\int_0^z \frac{\mathrm{d}z}{\sqrt{\Omega_m(1+z)^3 + 1 - \Omega_m}} \tag{9}
$$

is the theoretical luminosity distance in the flat ΛCDM model. Here $\mathcal{M}_c = (1+z)M\eta^{3/5}$ represents the observed chirp mass, where $M = m_1 + m_2$ is the total mass of binary components, and $\eta = m_1 m_2/M^2$ denotes the symmetric mass ratio. The expression of the function Ψ can be found in Zhao et al. (2011). Averaging the Fisher matrix over the inclination ι and the polarization ψ with the limit $\iota < 20°$ is nearly equivalent to taking $\iota = 0$. In the following simulations, we take the simplified case of $\iota = 0$, as Cai & Yang (2017) did in their treatment.

The combined signal-to-noise ratio (SNR) for the network of three independent ET interferometers is given by

$$
\rho = \sqrt{\sum_{i=1}^3 \langle \mathcal{H}^{(i)}, \mathcal{H}^{(i)}\rangle}, \tag{10}
$$

where the inner product is defined as

$$
\langle a,b\rangle = 4\int_{f_{\mathrm{lower}}}^{f_{\mathrm{upper}}} \frac{\tilde{a}(f)\tilde{b}^*(f)+\tilde{a}^*(f)\tilde{b}(f)}{2}\frac{\mathrm{d}f}{S_h(f)}, \tag{11}
$$

where $\sim$ represents the Fourier transformation, $S_h(f)$ is the one-side noise power spectral density characterizing the performance of the GW detector, f_{lower} and f_{upper} are the lower and upper cutoff frequencies. Here we adopt $f_{\mathrm{lower}} = 1$ Hz and $f_{\mathrm{upper}} = 2f_{\mathrm{LSO}}$, where the orbit frequency at the last stable orbit $f_{\mathrm{LSO}} = 1/(6^{3/2}2\pi M_{\mathrm{obs}})$ with the observed total mass

$M_{\mathrm{obs}} = (1+z)M$ (Zhao et al. 2011). The signal is claimed as a GW event only when the SNR of the detector network reaches over 8 (i.e., $\rho > 8.0$).

The instrumental uncertainty on the measurement of D_L^{GW} can be estimated by using the Fisher matrix. Assuming that the uncertainty of D_L^{GW} is irrelevant to the uncertainties of the remaining GW parameters, we have (Zhao et al. 2011)

$$
\sigma_{D_L}^{\mathrm{inst}} \simeq \sqrt{\left\langle \frac{\partial \mathcal{H}}{\partial D_L^{\mathrm{GW}}}, \frac{\partial \mathcal{H}}{\partial D_L^{\mathrm{GW}}}\right\rangle^{-1}}. \tag{12}
$$

As $\mathcal{H} \propto 1/D_L^{\mathrm{GW}}$, we can derive $\sigma_{D_L}^{\mathrm{inst}} \simeq D_L^{\mathrm{GW}}/\rho$. Considering the maximal effect of the inclination ι on the SNR, we add a factor of 2 to the instrumental uncertainty for a conservative estimation

$$
\sigma_{D_L}^{\mathrm{inst}} \simeq \frac{2D_L^{\mathrm{GW}}}{\rho}. \tag{13}
$$

We also add an additional error $\sigma_{D_L}^{\mathrm{lens}}/D_L^{\mathrm{GW}} = 0.05z$ due to the weak lensing effect. Thus, the total uncertainty on D_L^{GW} is taken to be

$$
\sigma_{D_L^{\mathrm{GW}}} = \sqrt{\left(\frac{2D_L^{\mathrm{GW}}}{\rho}\right)^2 + \left(0.05zD_L^{\mathrm{GW}}\right)^2}. \tag{14}
$$

3. MONTE CARLO SIMULATIONS

In this section, we perform Monte Carlo simulations to test how well GW standard sirens and cosmic chronometers can be used to constrain the cosmic curvature. To do so, we have to choose a fiducial cosmological model. Note that the exact value of the curvature parameter will not be essential in our simulations, since we are only interested in the precision with which it can be constrained. However, for consistency with current expansion rate measurements, we adopt their best-fit cosmological parameters in the fiducial flat ΛCDM model: $H_0 = 67.93$ km s^{-1} Mpc^{-1}, $\Omega_m = 0.324$, and $\Omega_\Lambda = 1 - \Omega_m$. Following the process of producing the mock GW data in Cai & Yang (2017), we expect the source redshift can be obtained by identifying an EM counterpart of the GW event, and simulate many catalogues of NS–NS and BH–NS systems with their z, D_L^{GW}, and $\sigma_{D_L}^{\mathrm{GW}}$. The redshift distribution of the observable sources is adopted as (Zhao et al. 2011)

$$
P(z) \propto \frac{4\pi D_C^2(z)R(z)}{H(z)(1+z)}, \tag{15}
$$

where $D_C(z)$ is the comoving distance, and $R(z)$ describes the time evolution of the burst rate, which is given by (Schneider et al. 2001; Cutler & Holz 2009)

$$
R(z) = \begin{cases} 1+2z, & z \le 1 \\ \frac{3}{4}(5-z), & 1 < z < 5 \\ 0, & z \ge 5. \end{cases} \tag{16}
$$

We sample the source redshift z from the probability distribution function (Equation (15)). To be consistent with the redshift range of current expansion rate measurements, we consider the potential observations of GW standard sirens in $0 < z < 2.0$. With the mock z, we calculate the fiducial value of D_L^{fid} based on Equation (9). The masses of each NS and BH are chosen to be uniform in the intervals $[1,2]$ and $[3,10]\ M_\odot$, respectively. The ratio of possibly detecting BH–NS and NS–NS events is assumed to be 0.03, as predicted
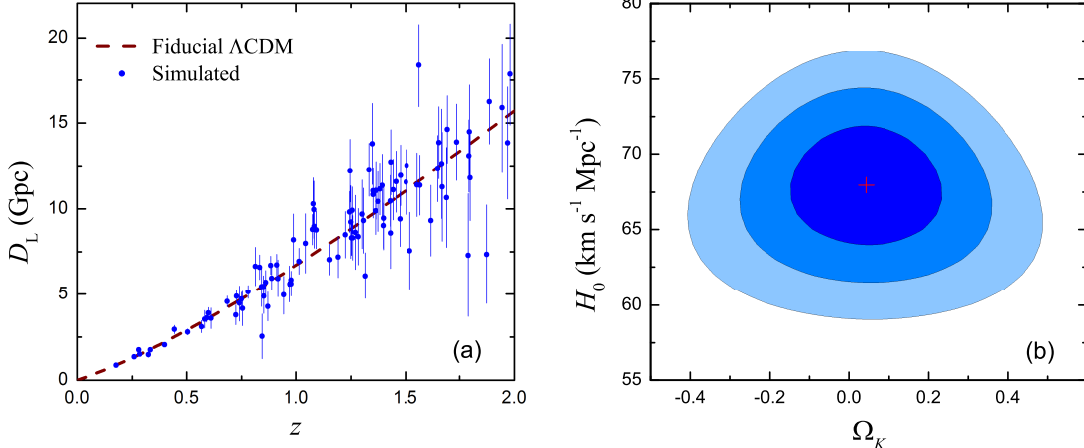
FIG. 2.— Panel (a): an example catalogue of 100 simulated GW events with redshifts z and luminosity distances D_L. The dashed line denotes the fiducial ΛCDM model. Panel (b): $1-3\sigma$ constraint contours for Ω_K and H_0, using 100 simulated GW events. The cross represents the best-fit pair.

for the Advanced LIGO-Virgo network (Abadie et al. 2010). The position angle θ is randomly sampled within the interval $[0, \pi]$.[3] We then evaluate the combined SNR for each set of the random values using Equation (10), and confirm that it is a successful GW event detection if $\rho > 8.0$. For every confirmed detection, we add the deviation $\sigma_{D_L^{GW}}$ in Equation (14) to the fiducial value of D_L^{fid}. That is, we sample the D_L^{GW} measurement according to the Gaussian distribution $D_L^{GW} = \mathcal{N}(D_L^{fid}, \sigma_{D_L^{GW}})$. The detection rates of BH–NS and NS–NS per year for the ET are estimated to be about the order $10^3 - 10^7$ events yr^{-1}. However, only a small fraction ($\sim 10^{-3}$) is predicted to have the observation of EM counterpart. Taking the detection rate in the middle rang $\mathcal{O}(10^5)$, and assuming that the fraction of the observation of EM counterpart is the same at any time interval, we can expect to detect $\mathcal{O}(10^2)$ GWs with EM counterparts per year. Note that we are only interested in what level of curvature constraints can be achieved by a certain number of future GW data together with their EM counterparts providing source redshifts. The use of the GW detection rate and the fraction of the observation of EM counterpart are therefore not essential in our simulations. We first simulate a population of 100 GW events with redshifts z, luminosity distances D_L^{GW}, and the errors of the luminosity distances $\sigma_{D_L^{GW}}$.

An example of 100 simulated GW events from the fiducial model is presented in Figure 2(a). By confronting distances $D_L^{GW}(z)$ from the simulated GW events with distances $D_L^H(z)$ in Equation (3) that depend on Ω_K and H_0 from observations of cosmic chronometers, we can obtain a model-independent estimation for the cosmic curvature by minimizing the χ^2 statistic:

$$\chi^2(\Omega_K, H_0) = \sum_i \frac{\left[D_L^H(z_i; \Omega_K, H_0) - D_L^{GW}(z_i) \right]^2}{\sigma^2_{D_L^H, i} + \sigma^2_{D_L^{GW}, i}} \, . \quad (17)$$

To ensure the final constraints are unbiased, we repeat the simulation process 1000 times for each data set by using different noise seeds. Figure 2(b) shows the constraint results on Ω_K and H_0.[4] We find that, from 100 simulated GW events and

<hr/>

[3] Because the SNR is independent of the other two angles ϕ and ψ, we do not need to consider them.

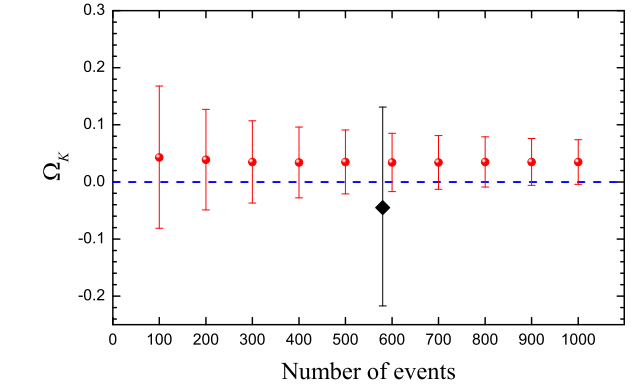[4] Here we use a Gaussian prior of $H_0 = 67.93 \pm 2.60$ km s^{-1} Mpc^{-1} to

FIG. 3.— Best-fit Ω_K and 1σ confidence level as a function of the number of GW events. The black diamond represents the model-independent constraint from 580 Union2.1 SNe Ia. The blue dashed line is the fiducial value.

observations of cosmic chronometers, the model-independent estimation for the cosmic curvature is $\Omega_K = 0.043^{+0.125}_{-0.124}$ (1σ). At this point, it is interesting to compare our forecast result with some actual model-independent tests involving the distances from other popular astrophysical probes. The error on the determined Ω_K is at the level of $\sigma_{\Omega_K} \simeq 0.125$ with 100 GW events, which is 40% smaller than that of the Union2.1/JLA SNe Ia ($\sigma_{\Omega_K} \simeq 0.20$; Li et al. 2016; Wei & Wu 2017a), and is 60% smaller than that of 120 radio quasars ($\sigma_{\Omega_K} \simeq 0.29$; Cao et al. 2017). Therefore, we can conclude that in the framework of model-independent methods testing the spatial curvature, GWs may achieve constraints with higher precision.

To better represent how effective our method might be with a certain number of GW events, in Figure 3 and Table 2 we display the best-fit Ω_K and 1σ confidence level as a function of the number of GW events N. The model-independent test of Ω_K from 580 Union2.1 SNe Ia (black diamond; Li et al. 2016) is also plotted for comparison. One can see from Figure 3 that as the number of GW events increases, the uncertainty of Ω_K is reduced. The precision of the determined Ω_K from 100 GW events is already better than that of 580 Union2.1 SNe Ia. The spatial curvature can be constrained with an error of only 0.04 if 1000 GW events are observed.

By the time we have ET results, there might be other $H(z)$

guide the minimization procedure over H_0.

TABLE 2
SUMMARY OF MODEL-INDEPENDENT CURVATURE DETERMINATIONS
FROM N SIMULATED GW EVENTS AND OBSERVATIONS OF COSMIC
CHRONOMETERS

N^a	Ω_K	N^a	Ω_K
100	$0.043^{+0.125}_{-0.124}$	600	0.034 ± 0.051
200	0.039 ± 0.088	700	0.034 ± 0.047
300	0.035 ± 0.072	800	0.035 ± 0.044
400	0.034 ± 0.062	900	0.035 ± 0.041
500	0.035 ± 0.056	1000	0.035 ± 0.039

$^a N$ denotes the number of GW events.

measurements with wider redshift range and higher accuracy from different observables. To investigate the case of adding more cosmic-chronometer measurements, we also perform Monte Carlo simulations to create the mock $H(z) - z$ data sets. We assume that there are other 50 mock $H(z) - z$ data points by the time that 1000 GW events are detected, the redshifts of which are chosen equally in $\log(1+z)$ space in $0.1 \leq z \leq 5.0$. The relative uncertainty of these mock data is taken at a level of 1%, which will be realized in future observations (Weinberg et al. 2013). The route of GW simulation is the same as described earlier in Section 3, but now we consider the potential observations of GW standard sirens in $0 < z < 5.0$. Figure 4 gives an example of the simulations in the case of adding 50 cosmic-chronometer measurements. From top to bottom, the three panels show the cosmic-chronometer data (including 31 observed $H(z)$ data (solid points) and 50 mock $H(z)$ data (circles)) with the reconstructed $H(z)$ function (solid line), the reconstructed $D_C(1+z)$ function (solid line) and 1000 simulated GW events with luminosity distances D_L (solid points), and the final constraints on Ω_K and H_0, respectively. In this case, the final derived Ω_K is $\Omega_K = -0.002 \pm 0.028$ (1σ). Compared with the constraint obtained from 1000 simulated GW events and 31 current cosmic-chronometer measurements ($\Omega_K = 0.035 \pm 0.039$), the uncertainty of the determined Ω_K in this case can be further improved by a factor of 1.4.

4. SUMMARY AND DISCUSSION

The coincident detection of gravitational and EM waves from a binary NS merger has formally opened a new window on observational cosmology. More precisely, the greatest advantage of GW standard sirens is that the distance calibration is independent of any other distance ladders. In this work, we investigate the constraint ability of future GW observations of the ET on the spatial curvature by using a model-independent method. The main principle of our method is to compare two kinds of luminosity distances. One distance $D_L^H(\Omega_K, H_0)$ is constructed with Hubble parameter measurements obtained from observations of cosmic chronometers, which is susceptible to the curvature parameter Ω_K and the Hubble constant H_0. Based on the discrete Hubble parameter data, we first use the GP method to reconstruct the continuous $H(z)$ function. Next, we obtain the model-independent comoving distance function $D_C(z)$ by directly calculating the integral of the reconstructed $H(z)$ function. Using this continuous $D_C(z)$ function, the luminosity distance $D_L^H(\Omega_K, H_0)$ from the $H(z)$ measurements can be further calculated at a certain z. The other distance D_L^{GW} is from the simulated GW data, which is independently determined. Previously, by confronting $D_L^H(\Omega_K, H_0)$ with luminosity distances from observations of SNe Ia, some studies achieved model-independent constraints on the spatial curvature (Li et al. 2016; Wei & Wu 2017a). However, the con-
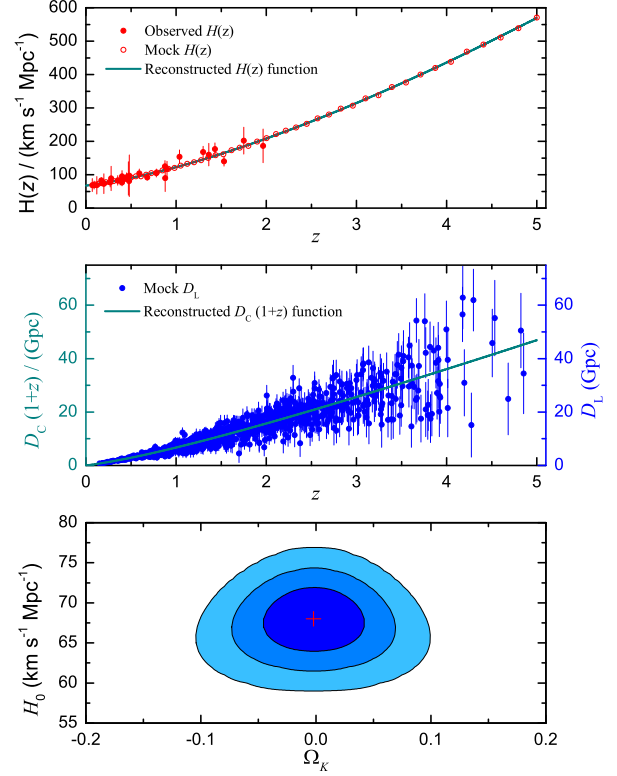

FIG. 4.— An example of the simulations for the case of 81 cosmic-chronometer measurements and 1000 simulated GW events. Top panel shows the cosmic-chronometer data (including 31 observed $H(z)$ data (solid points) and 50 mock $H(z)$ data (circles)) with the reconstructed $H(z)$ function (solid line). Middle panel shows the reconstructed $D_C(1+z)$ function (solid line) and 1000 mock D_L data (solid points). Bottom panel shows the final constraints on Ω_K and H_0 from these data.

straint ability of SNe Ia are obviously restricted by the fact that their distances depend on light-curve fitting parameters. While GW standard sirens have the advantage of being self-calibrating. Therefore, combining the GW observations with $H(z)$ data may provide a powerful and novel way to estimate the spatial curvature.

Through Monte Carlo simulations, we find that the error of the curvature parameter can be expected to be constrained at the level of ~ 0.125 by combining 31 current observed $H(z)$ data and 100 simulated GW data. The uncertainty of Ω_K can be further reduced to ~ 0.04 if 1000 GW events are observed. We also find that with 81 cosmic-chronometer measurements (including 31 observed $H(z)$ data and 50 mock $H(z)$ data) and 1000 simulated GW events, one can expect the zero cosmic curvature to be estimated at the precision of $\Omega_K = -0.002 \pm 0.028$. By comparing our results with previous ones which reported model-independent curvature tests using current data of SNe Ia and radio quasars (Li et al. 2016; Cao et al. 2017; Wei & Wu 2017a), we demonstrate that future measurements of the luminosity distances of GW sources will be more competitive than current analyses. These results show that the prospects for testing the spatial curvature with GW observations is very promising.

REFERENCES

Abadie, J., Abbott, B. P., Abbott, R., et al. 2010, Nuclear Instruments and Methods in Physics Research A, 624, 223

Abbott, B. P., Abbott, R., Abbott, T. D., et al. 2017a, Physical Review Letters, 119, 161101

Abbott, B. P., Abbott, R., Abbott, T. D., et al. 2017b, Nature, 551, 85

Bernstein, G. 2006, ApJ, 637, 598

Bilicki, M., & Seikel, M. 2012, MNRAS, 425, 1664

Boehm, C., & Räsänen, S. 2013, JCAP, 9, 003

Cai, R.-G., Guo, Z.-K., & Yang, T. 2016, Phys. Rev. D, 93, 043517

Cai, R.-G., Liu, T.-B., Liu, X.-W., Wang, S.-J., & Yang, T. 2018, Phys. Rev. D, 97, 103005

Cai, R.-G., & Yang, T. 2017, Phys. Rev. D, 95, 044024

Cao, S., Qi, J., Biesiada, M., et al. 2017, ArXiv e-prints, arXiv:1708.08608

Chen, Y., Ratra, B., Biesiada, M., Li, S., & Zhu, Z.-H. 2016, ApJ, 829, 61

Clarkson, C., Bassett, B., & Lu, T. H.-C. 2008, Physical Review Letters, 101, 011301

Clarkson, C., Cortês, M., & Bassett, B. 2007, JCAP, 8, 011

Coulter, D. A., Foley, R. J., Kilpatrick, C. D., et al. 2017, Science, 358, 1556

Cutler, C., & Holz, D. E. 2009, Phys. Rev. D, 80, 104009

Del Pozzo, W. 2012, Phys. Rev. D, 86, 043011

Del Pozzo, W., Li, T. G. F., & Messenger, C. 2017, Phys. Rev. D, 95, 043502

Denissenya, M., Linder, E. V., & Shafieloo, A. 2018, JCAP, 3, 041

Eisenstein, D. J., Zehavi, I., Hogg, D. W., et al. 2005, ApJ, 633, 560

Enqvist, K. 2008, General Relativity and Gravitation, 40, 451

Farooq, O., Mania, D., & Ratra, B. 2015, Ap&SS, 357, 11

Farooq, O., Ranjeet Madiyar, F., Crandall, S., & Ratra, B. 2017, ApJ, 835, 26

Ferrer, F., Multamäki, T., & Räsänen, S. 2009, Journal of High Energy Physics, 4, 006

Ferrer, F., & Räsänen, S. 2006, Journal of High Energy Physics, 2, 016

Goldstein, A., Veres, P., Burns, E., et al. 2017, ApJ, 848, L14

Gong, Y., & Wang, A. 2007, Phys. Rev. D, 75, 043520

Gott, III, J. R. 1982, Nature, 295, 304

Hawking, S. W. 1984, Nuclear Physics B, 239, 257

Hogg, D. W. 1999, ArXiv Astrophysics e-prints, astro-ph/9905116

Holz, D. E., & Hughes, S. A. 2005, ApJ, 629, 15

Ichikawa, K., Kawasaki, M., Sekiguchi, T., & Takahashi, T. 2006, JCAP, 12, 005

Ichikawa, K., & Takahashi, T. 2006, Phys. Rev. D, 73, 083526

Jimenez, R., & Loeb, A. 2002, ApJ, 573, 37

Jimenez, R., Verde, L., Treu, T., & Stern, D. 2003, ApJ, 593, 622

Jimenez, R., Raccanelli, A., Verde, L., & Matarrese, S. 2018, JCAP, 4, 002

Knox, L. 2006, Phys. Rev. D, 73, 023503

Lavinto, M., Räsänen, S., & Szybka, S. J. 2013, JCAP, 12, 051

L'Huillier, B., & Shafieloo, A. 2017, JCAP, 1, 015

Li, Y.-L., Li, S.-Y., Zhang, T.-J., & Li, T.-P. 2014, ApJ, 789, L15

Li, Z., Ding, X., Wang, G.-J., Liao, K., & Zhu, Z.-H. 2018, ApJ, 854, 146

Li, Z., Wang, G.-J., Liao, K., & Zhu, Z.-H. 2016, ApJ, 833, 240

Liao, K., Li, Z., Wang, G.-J., & Fan, X.-L. 2017a, ApJ, 839, 70

Liao, K., Fan, X.-L., Ding, X., Biesiada, M., & Zhu, Z.-H. 2017b, Nature Communications, 8, 1148

Lin, H.-N., Li, J., & Li, X. 2018, European Physical Journal C, 78, 356

Melia, F., & Yennapureddy, M. K. 2018, JCAP, 2, 034

Messenger, C., Takami, K., Gossan, S., Rezzolla, L., & Sathyaprakash, B. S. 2014, Physical Review X, 4, 041004

Mitra, S., Choudhury, T. R., & Ratra, B. 2017, ArXiv e-prints, arXiv:1712.00018

Moresco, M. 2015, MNRAS, 450, L16

Moresco, M., Verde, L., Pozzetti, L., Jimenez, R., & Cimatti, A. 2012, JCAP, 7, 053

Moresco, M., Pozzetti, L., Cimatti, A., et al. 2016, JCAP, 5, 014

Mortsell, E., & Jonsson, J. 2011, ArXiv e-prints, arXiv:1102.4485

Nissanke, S., Holz, D. E., Hughes, S. A., Dalal, N., & Sievers, J. L. 2010, ApJ, 725, 496

Ooba, J., Ratra, B., & Sugiyama, N. 2017a, ArXiv e-prints, arXiv:1707.03452

Ooba, J., Ratra, B., & Sugiyama, N. 2017b, ArXiv e-prints, arXiv:1710.03271

Ooba, J., Ratra, B., & Sugiyama, N. 2017c, ArXiv e-prints, arXiv:1712.08617

Park, C.-G., & Ratra, B. 2018a, ArXiv e-prints, arXiv:1801.00213

Park, C.-G., & Ratra, B. 2018b, ArXiv e-prints, arXiv:1803.05522

Planck Collaboration, Ade, P. A. R., Aghanim, N., et al. 2016, A&A, 594, A13

Qi, J.-Z., Cao, S., Zhang, S., et al. 2018, ArXiv e-prints, arXiv:1803.01990

Rana, A., Jain, D., Mahajan, S., & Mukherjee, A. 2017, JCAP, 3, 028

Räsänen, S. 2009, JCAP, 2, 011

Räsänen, S., Bolejko, K., & Finoguenov, A. 2015, Physical Review Letters, 115, 101301

Ratra, B. 1985, Phys. Rev. D, 31, 1931

Ratra, B. 2017, Phys. Rev. D, 96, 103534

Ratra, B., & Peebles, P. J. E. 1994, ApJ, 432, L5

Ratra, B., & Peebles, P. J. E. 1995, Phys. Rev. D, 52, 1837

Ratsimbazafy, A. L., Loubser, S. I., Crawford, S. M., et al. 2017, MNRAS, 467, 3239

Redlich, M., Bolejko, K., Meyer, S., Lewis, G. F., & Bartelmann, M. 2014, A&A, 570, A63

Ryan, J., Doshi, S., & Ratra, B. 2018, ArXiv e-prints, arXiv:1805.06408

Sapone, D., Majerotto, E., & Nesseris, S. 2014, Phys. Rev. D, 90, 023012

Sathyaprakash, B. S., & Schutz, B. F. 2009, Living Reviews in Relativity, 12, 2

Sathyaprakash, B. S., Schutz, B. F., & Van Den Broeck, C. 2010, Classical and Quantum Gravity, 27, 215006

Schneider, R., Ferrari, V., Matarrese, S., & Portegies Zwart, S. F. 2001, MNRAS, 324, 797

Schutz, B. F. 1986, Nature, 323, 310

Seikel, M., Clarkson, C., & Smith, M. 2012a, JCAP, 6, 036

Seikel, M., Yahya, S., Maartens, R., & Clarkson, C. 2012b, Phys. Rev. D, 86, 083001

Shafieloo, A., & Clarkson, C. 2010, Phys. Rev. D, 81, 083537

Simon, J., Verde, L., & Jimenez, R. 2005, Phys. Rev. D, 71, 123001

Stern, D., Jimenez, R., Verde, L., Kamionkowski, M., & Stanford, S. A. 2010, JCAP, 2, 008

Takada, M., & Doré, O. 2015, Phys. Rev. D, 92, 123518

Tegmark, M., Eisenstein, D. J., Strauss, M. A., et al. 2006, Phys. Rev. D, 74, 123507

Virey, J.-M., Talon-Esmieu, D., Ealet, A., Taxil, P., & Tilquin, A. 2008, JCAP, 12, 008

Wang, G.-J., Wei, J.-J., Li, Z.-X., Xia, J.-Q., & Zhu, Z.-H. 2017, ApJ, 847, 45

Wang, L.-F., Zhang, X.-N., Zhang, J.-F., & Zhang, X. 2018, ArXiv e-prints, arXiv:1802.04720

Wei, J.-J., & Wu, X.-F. 2017a, ApJ, 838, 160

Wei, J.-J., & Wu, X.-F. 2017b, MNRAS, 472, 2906

Wei, J.-J., Wu, X.-F., & Gao, H. 2018, ApJ, 860, L7

Weinberg, D. H., Mortonson, M. J., Eisenstein, D. J., et al. 2013, Phys. Rep., 530, 87

Witzemann, A., Bull, P., Clarkson, C., et al. 2018, MNRAS, 477, L122

Wright, E. L. 2007, ApJ, 664, 633

Xia, J.-Q., Yu, H., Wang, G.-J., et al. 2017, ApJ, 834, 75

Yahya, S., Seikel, M., Clarkson, C., Maartens, R., & Smith, M. 2014, Phys. Rev. D, 89, 023503

Yang, T., Holanda, R. F. L., & Hu, B. 2017, ArXiv e-prints, arXiv:1710.10929

Yennapureddy, M. K., & Melia, F. 2017, JCAP, 11, 029

Yennapureddy, M. K., & Melia, F. 2018, European Physical Journal C, 78, 258

Yu, H., Ratra, B., & Wang, F.-Y. 2018, ApJ, 856, 3

Yu, H., & Wang, F. Y. 2016, ApJ, 828, 85

Zhang, C., Zhang, H., Yuan, S., et al. 2014, Research in Astronomy and Astrophysics, 14, 1221

Zhao, G.-B., Xia, J.-Q., Li, H., et al. 2007, Physics Letters B, 648, 8

Zhao, W., van den Broeck, C., Baskaran, D., & Li, T. G. F. 2011, Phys. Rev. D, 83, 023005

Zhao, W., & Wen, L. 2018, Phys. Rev. D, 97, 064031

Zhao, W., Wright, B. S., & Li, B. 2018, ArXiv e-prints, arXiv:1804.03066

Zolnierowski, Y., & Blanchard, A. 2015, Phys. Rev. D, 91, 083536